Metallic Hydrides I: Hydrogen Storage and Other Gas-Phase Applications

Robert C. Bowman Jr. and Brent Fultz

Abstract

A brief survey is given of the various classes of metal alloys and compounds that are suitable for hydrogen-storage and energy-conversion applications. Comparisons are made of relevant properties including hydrogen absorption and desorption pressures, total and reversible hydrogen-storage capacity, reaction-rate kinetics, initial activation requirements, susceptibility to contamination, and durability during long-term thermal cycling. Selected applications are hydrogen storage as a fuel, gas separation and purification, thermal switches, and sorption cryocoolers.

Keywords: *hydrogen storage, metal hydrides, neutron scattering.*

Introduction

In the late 1960s, it was discovered that certain intermetallic compounds (e.g., Mg_2Ni, $LaNi_5$, and TiFe) would directly and reversibly react with hydrogen gas at practical temperatures (i.e., 250–650 K). These observations, coupled with the petroleum embargoes and related energy crises of the 1970s, stimulated extensive investigations on metal hydrides for energy storage and conversion.[1,2] While many intermetallic hydrides can absorb substantial quantities of hydrogen (i.e., hydrogen-to-metal atom ratios >1), most of these alloys composed of rare-earth or transition metals have a maximum storage of about ~1–2% hydrogen by weight. Alloys of Mg are an exception, having hydrogen capacities in the range of 3.3–7.7 wt%.[3,4] Hundreds of intermetallic alloys have been screened for hydrogen-storage potential[5,6] with respect to the following criteria:

- reversible hydrogen capacity,
- operating pressure/temperature range,
- reaction kinetics,
- degradation after repeated cycling of hydrogen, and
- cost.

The search continues for the "Holy Grail" of hydrides that will excel at all of these requirements. Recently, this quest has been expanded to include light-metal complex hydrides such as catalyzed alanates[6] (ternary compounds containing AlH_4) and nanostructured carbon materials, as described in the article by Bogdanović and Sandrock in this issue of *MRS Bulletin.*

Properties of Metal Hydrides

The desired reaction for a generic intermetallic alloy AB_z with hydrogen gas is

$$AB_z + xH_2 = AB_zH_{2x} + \Delta Q, \qquad (1)$$

where ΔQ is the heat released upon absorption of hydrogen.

Typically, metal A forms stable binary hydrides, that is, A is an early transition metal, rare-earth metal, or Mg. Metal B (e.g., Ni, Co, Cr, Fe, Mn, or Al) does not form stable hydrides, although it may help dissociate the H_2 molecule. Table I describes representative hydrides from the five metal hydride families (i.e., A, A_2B, AB, AB_2, and AB_5) that have shown the most promise[6] for practical hydrogen storage. The heat ΔQ released upon absorption is usually characterized by the enthalpy parameter ($\Delta H_{plateau}$) determined from a van't Hoff plot of the equilibrium pressures in the middle of the plateau regions (i.e., plateau pressures) of the pressure–composition–temperature (PCT) isotherms.[6] Key hydrogen-storage properties for these examples are summarized in the table. Both the total hydrogen capacity and the reversible portion are presented in weight percentage of hydrogen. There are often considerable differences between these quantities when hydride phases vary greatly in stability, as in VH_x and $ZrNiH_x$. The average desorption pressure (P_{des}) at room temperature and the temperature where P_{des} = 1.013 bar are also listed in the table. To be considered for fuel storage in a vehicle powered by either fuel cells or an internal-combustion engine, it is generally accepted that the hydrides should provide hydrogen gas at ~1–10 bar over the temperature range from 270 K to upper limits between ~360 K and 600 K, depending on the availability of a source of heat. The hydrides of ZrNi, $ZrMn_2$, or the Mg alloys are therefore unsuitable for these applications. While the other alloys in Table I can provide adequate gas pressure at reasonable operating temperatures, their reversible capacity is less than 2 wt%, which would probably translate to an unacceptably large mass for a convenient personal transportation vehicle (i.e., a passenger car).

Most metallic hydrides are nonstoichiometric interstitial compounds with hydrogen occupying either the tetrahedral $A_{4-x}B_x$ or octahedral $A_{6-x}B_x$ interstices. It has become widely recognized that two factors strongly influence which interstitial sites in the metal host lattice can accommodate hydrogen: (1) the site radius needs to be at least ~0.040 nm, and (2) occupied sites should be separated by at least ~0.21 nm. Since this separation is comparable to the spacing between metal atoms, it is very unusual to find ternary hydrides with maximum H/M ratios above 1.5; most are closer to ~1. There are a few cases of higher ratios, but these hydrides are too expensive (i.e., $BaReH_9$ or $NaKReH_9$) or have 1-bar desorption temperatures above 600 K (i.e., the Mg compounds).

Performance

When developing a practical hydride for any given application, a large number of properties beyond storage capacity and PCT values need to be considered.[5] These include inefficiencies induced by hysteresis[6] between the absorption and desorption pressure, ease of initial hydriding or activation, sensitivity to air or other gas impurities, volume expansion, decrepitation into fine powder during hydrogen adsorption/desorption cycling, and safety factors such as pyrophoricity or toxicity. Here, we discuss two other important

Table I: Key Properties of Metal Hydrides Suitable for Gas-Phase Applications.

Alloy Type	Crystal Structure Type	Hydride Phase	Maximum H Capacity (wt%)	Reversible H Capacity (wt%)	P_{des}[a] at 298 K (bar)	T (K) for 1.013 bar P_{des}	$-\Delta H_{plateau}$[b] (kJ/mol H_2)	Comments
A	*A*3 (*hP*2)	MgH_2	7.66	<7.0	$\sim 10^{-6}$	552	74.5	Ni improves kinetics
A	*A*2 (*cI*2)	VH_2	3.81	1.9	2.1	285	40.1	Two plateaus, difficult to activate
A_2B	C_a (*hP*18)	Mg_2NiH_4	3.59	3.3	$\sim 10^{-5}$	528	64.5	Not metallic, very slow kinetics for $T < 500$ K
AB	*B*2 (*cP*2)	$TiFeH_2$	1.89	1.5	4.1	265	28.1	Two plateaus, hard to activate
AB	*Bf* (*oC*8)	$ZrNiH_3$	1.96	1.1	$\sim 5 \times 10^{-6}$	573	68.6	Two plateaus, fast kinetics
AB_2	*C*14 (*hP*12)	$TiMn_{1.4}V_{0.62}H_{3.4}$	2.15	1.1	3.6	268	28.6	V makes it more expensive
AB_2	*C*14 (*hP*12)	$ZrMn_2H_{3.6}$	1.77	0.9	0.001	440	53.2	Powder is highly pyrophoric
AB_5	D_{2d} (*hP*6)	$LaNi_5H_{6.5}$	1.49	1.28	1.8	285	30.8	Fast kinetics, but degrades for $T > \sim 350$ K
AB_5	D_{2d} (*hP*6)	$LaNi_{4.8}Sn_{0.2}H_{6.0}$	1.40	1.24	0.5	312	32.8	Slow degradation for $T < 550$ K

Note: After Reference 6.
[a] P_{des} is the average desorption pressure.
[b] $\Delta H_{plateau}$ is the enthalpy of the plateau region of the hydride PCT isotherms (negative quantity for exothermic reactions).

properties: factors that determine reaction kinetics, and hydride stability during cyclic operation.

Numerous factors can contribute to the kinetics of the forward and reverse reactions in Equation 1. In many engineering applications,[2] it is the heat transfer either into or from the hydride powder during desorption or absorption that controls the process. This factor is especially important when large amounts of gas are involved or a rapid transfer of gas is demanded between heating and cooling beds. It can be a major engineering challenge to enhance heat conductivity for the hydride powder without excessively increasing the mass and size of its container.[2] The kinetics of the hydrogen reactions at the alloy surfaces can also establish the hydriding rates, especially if there are stable oxide layers or contaminating species in the hydrogen gas. One of the best advantages of the AB_2 alloys and especially the AB_5 alloys is the selective oxidation and segregation of the A metal at the surface, leaving a catalytic B species at the surface to promote adsorption and dissociation of the hydrogen molecules.[7] The final contributor to kinetics is the hydrogen-diffusion rate within the alloy and hydride phases. Figure 1 shows the intrinsic diffusion coefficients (D) for representative hydrides, obtained mostly by nuclear magnetic resonance[8] or quasi-

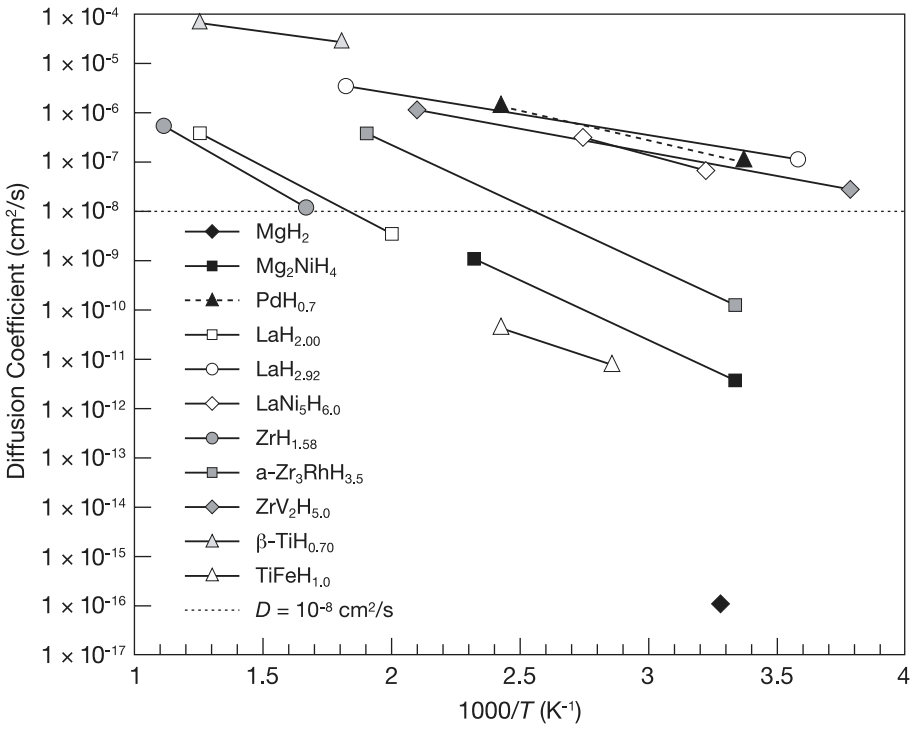

Figure 1. Intrinsic diffusion coefficients (D) *for representative metal hydrides, obtained mostly by nuclear magnetic resonance[8] or quasi-elastic neutron scattering.[8] The* D *value for MgH_2 was from an x-ray photoelectron spectroscopy study by Spatz et al.[9] The horizontal dotted line at* $D = 1 \times 10^{-8}$ *represents the approximate conditions of a hydrogen atom diffusing 10 μm in 10 s.*

elastic neutron scattering.[8] The D value for MgH_2 was from an x-ray photoelectron spectroscopy study by Spatz et al.[9] When $D = 1.7 \times 10^{-8}$ cm^2/s, the mean time ($d^2/6D$) for a hydrogen atom to diffuse $d = 10$ μm is 10 s. Since the particle dimensions of most activated metal hydrides are in the range of 1–100 μm, complete transport of hydrogen through these particles would normally occur within a minute or so. Bulk diffusion should be adequate for $PdH_{0.7}$, $LaH_{2.92}$, β-$TiH_{0.7}$, $LaNi_5H_6$, and ZrV_2H_5 at temperatures above 250 K, or above ~600 K for $ZrH_{1.58}$ or $LaH_{2.0}$. However, the diffusion coefficients for $TiFeH_1$ and Mg_2NiH_4 are sufficiently small below 400 K that bulk diffusion within these hydrides certainly controls reaction kinetics. The situation is most unfortunate for MgH_2, where diffusion limits the reaction rates, even for nanocrystalline particles.[4]

If a very stable binary hydride AH_x exists, the AB_zH_{2x} hydride of Equation 1 is usually metastable and will tend to disproportionate into AH_x and additional B-enriched compounds or hydrides.[5,6,10,11] The disproportionation reaction requires the diffusion of metal atoms, so its impact is usually small around room temperature. When the ternary hydrides are cycled to elevated temperatures for desorption of gas, however, disproportionation can cause losses in reversible storage capacity and degrade the PCT curves.[10,11] This problem is particularly severe for hydrides of the $LaNi_5$ alloys. As shown in Figure 2, the partial substitution of some of the Ni by Sn greatly reduces the rate of degradation from disproportionation.[10] Similar improvements have been found for Al, Ge, and Si substitution. Furthermore, degradation from disproportionation can usually be reversed by vacuum annealing at $T > 600$ K, since disproportionation does not involve the formation of irreversible phases such as oxides or carbides, which are common during contamination reactions.[5] There have been very few studies on the behavior of the ABH_x and AB_2H_x systems during temperature cycling. Wanner et al.[11,12] have reported that $Ti_{0.98}Zr_{0.02}V_{0.43}Fe_{0.09}Mn_{1.5}H_{1.95}$ had only a 6% loss in capacity after 85,100 cycles between 318 K and 393 K, while Lee and Lee[13] found a 22% capacity loss from $Zr_{0.9}Ti_{0.1}Cr_{0.9}Fe_{1.1}H_{3.2}$ after just 1200 cycles between 298 K and 593 K. Enhanced diffusion rates of the host metal atoms at increasing temperature will promote phase segregation and the disproportionation reaction.

Alloy Design

An important feature of the AB_5 and AB_2 alloys (and to a lesser extent the AB alloys) is that their operating pressures and temperatures can be adjusted through solute substitution for both A and B metals. The plateau pressures at a selected temperature can often be changed by more than two orders of magnitude. In general, the larger the lattice parameters of the host alloy, the lower the pressure. Deviations in the alloy composition (i.e., changes in the B/A ratios) also lead to significant changes in the PCT parameter,[14] which can be advantageous in many situations.[1,2,6] Unfortunately, both of these alloy variations usually result in a smaller hydrogen-storage capacity than pure stoichiometric binary AB_z intermetallics. This effect is illustrated in Figure 3 for the hexagonal $C14$ Laves-phase AB_2 alloy $ZrMn_x$ ($1.8 < x < 3$), where mid-plateau absorption pressures[15] vary by nearly a factor of 50 over these compositions. A large capacity and the smallest plateau slopes occur for the stoichiometric alloy $ZrMn_2$. Hysteresis was independent of x. It should be noted that the isotherms for many AB_2 hydrides exhibit large slopes in their plateaus, due to either reduction in their critical temperature[6] or large variations of the local hydrogen environments from both substitution and composition disorder.

Researchers in France, Japan, and elsewhere have recently observed that the presence of secondary phases often greatly improves the activation behavior and reaction kinetics of AB_2 alloys during both electrochemical charging and gas-phase charging.[16–18] The precipitation of A, AB, or A_7B_{10} phases seems to occur mainly between crystallites of the host alloy and facilitates the transfer of hydrogen across particle interfaces. While the formation of these impurity phases can degrade the PCT properties by altering the host composition, the effect on storage capacity is usually minor. These multiphase alloys exhibit greatly enhanced overall performance as compared with similar single-phase hydrides.[17] The secondary phases exhibit a wide range of structural transitions upon hydriding and sometimes become amorphous.[18]

There is a broad consensus that high surface areas are detrimental to cycle life (especially in electrochemical cells[19,20]). The breakup of $LaNi_5$ particles during hydrogen absorption/desorption cycling increases the surface area, promoting surface reactions and diffusion. This breakup, or "decrepitation," is often attributed to the strains in $LaNi_5$ from lattice expansion and two-phase coexistence during hydriding, which are enormous, being 5–7%. The elastic limit of brittle $LaNi_5$ is well below 1%, and with abundant flaws in the material, it seems intuitive that cracking should occur. Nevertheless, the beneficial solute additions do not suppress the volume dilatations of hydriding anywhere near to what is required to reduce the hydriding strains below the elastic limit of $LaNi_5$. Furthermore, the volume dilatation of hydriding, if constant throughout the material, cannot directly affect the decrepitation of the metal hydride. If the volume dilatation of hydriding is large, but occurs uniformly throughout the material, there can be no release of elastic energy by crack propagation.

The homogeneity of hydrogen distributions was measured recently in a small-angle neutron scattering (SANS) study on deuterided $LaNi_5$ and $LaNi_{4.75}Sn_{0.25}$.[21] Figure 2 shows that the $LaNi_{4.8}Sn_{0.2}$ alloy has a superior cycle life to $LaNi_5$ in gas-phase reactions[10] (and also in electrochemical cells[22]). Associated x-ray diffractometry of hydrided materials showed that the overall volume expansions of the two alloys

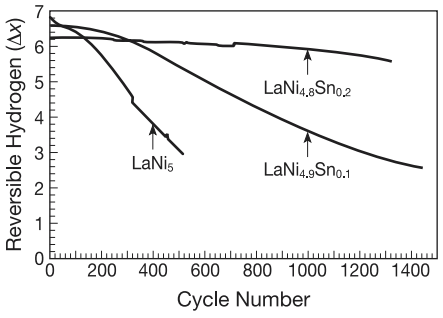

Figure 2. Effect of Sn substitution on the reversible hydrogen-storage capacity of $LaNi_{5-x}Sn_x$ hydrides after cycling between 295 K and 510 K. (After Reference 10.)

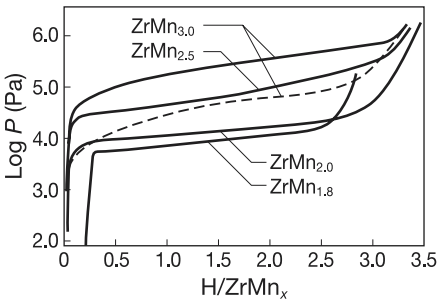

Figure 3. Effect of alloy stoichiometry on the absorption pressures (solid lines) for the C14 Laves-phase alloy $ZrMn_x$. An example of hysteresis is shown by the desorption curve (dashed line) for the composition $ZrMn_3$. (After Reference 15.)

were approximately the same: $LaNi_5$ and $LaNi_{4.75}Sn_{0.25}$ had differences of 23% and 21%, respectively, in unit-cell volumes between fully hydrided and fully dehydrided states. The unit cell of the hydride phase in $LaNi_{4.75}Sn_{0.25}$ shrinks continuously with dehydriding, as opposed to that of $LaNi_5$. For $LaNi_5$ (Figure 4a), the peaks from the two phases remain in approximately the same position, but change their intensity as hydrogen is lost from the material. On the other hand, for $LaNi_{4.75}Sn_{0.25}$ (Figure 4b), the diffraction peaks from the hydride phase shift to higher angles during the loss of hydrogen, showing a continuous reduction in lattice parameter. SANS measurements performed on deuterided samples of both $LaNi_5$ and $LaNi_{4.75}Sn_{0.25}$ showed that the deuterium distribution was more heterogeneous in partially deuterided $LaNi_5$. The two alloys had nearly identical SANS profiles before deuteriding, and Figure 5a shows SANS curves that are nearly identical when both are fully deuterided. This is expected, since with the occupancy of all available sites for hydrogen, the hydrogen must be uniform throughout the whole material. More interesting is the difference in the two SANS profiles shown in Figure 5b. The curves for $LaNi_{4.75}Sn_{0.25}D_2$ are essentially the same as those of $LaNi_{4.75}Sn_{0.25}D_6$ in Figure 5a, indicating that at partial deuteriding, the deuterium distribution is uniform throughout the material. On the other hand, the partially deuterided samples of $LaNi_5D_x$ have different SANS profiles. The deuterium in $LaNi_5D_2$ is not homogeneous in the alloy.

The spatial scales of these hydrided zones, or rather the correlation length for the hydrogen-density fluctuations in partially hydrided binary $LaNi_5$, are of the order of 100 Å. With a linear strain of 5–7% from full hydriding, the variation of hydrogen concentration from 0% to 100% over a distance of 100 Å results in a large strain gradient that could lead to the generation of dislocations or other crystalline defects of significance to mechanical properties. This smoothing of the mesoscopic hydrogen-concentration profile may be why $LaNi_{5-x}Sn_x$ alloys sustain less microstructural damage than binary $LaNi_5$. The more homogeneous hydrogen distribution promoted by alloying with Sn could be responsible for the improved cycle life of solute-modified $LaNi_5$ for both gas storage and as an electrode material for electrochemical cells.

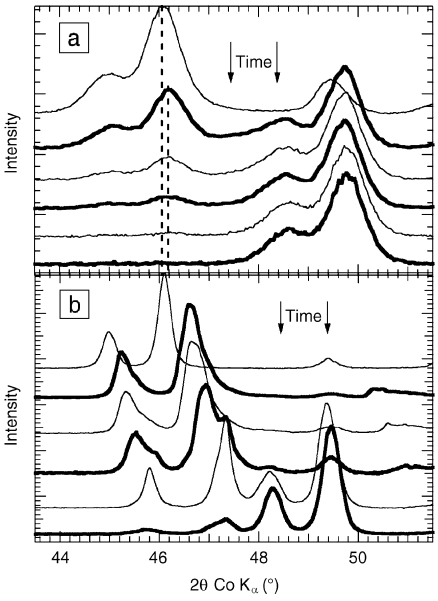

Figure 4. X-ray diffraction (XRD) patterns of (a) binary $LaNi_5$ and (b) ternary $LaNi_{4.75}Sn_{0.25}$ containing various amounts of hydrogen. In these figures, the diffraction pattern from the fully hydrided material is at top, and the lower patterns were measured after increasing amounts of hydrogen loss. Notice that only the β phase (between $2\theta = 45°$ and 47°) of the ternary $LaNi_{4.75}Sn_{0.25}$ alloy shows any continuous variation with hydrogen desorption. (After Reference 21.) Alternating bold and plain traces are for visual discrimination of adjacent XRD patterns.

Gas-Phase Applications of Metal Hydrides

In contrast to the widespread commercialization of Ni-MH batteries during the past decade, gas-phase applications of metal hydrides have not reached the same level of commercial importance. Table II provides an overview of major types of energy storage and conversion applications for the hydrides that have been investigated. Mandatory hydride properties for each type of application are briefly summarized, along with important secondary issues and candidate alloys. More complete descriptions of these applications, as well as their requirements for hydride properties, can be readily found in previous reviews.[1,2,5,6] Since the release rate of gas from a hydride bed is limited by an endothermic desorption process, researchers have always[1,2] claimed metal hydrides to be much safer than either high-pressure hydrogen gas or liquid hydrogen for storage in transportation. There have been several demonstrations since the 1970s of various types of vehicles (i.e., automobiles, pickup trucks, vans, tractors, and buses) in the United States, Germany, and Japan using metal-hydride fuel storage for internal-combustion engines.[2] While the feasibility of hydride storage has clearly been established, various engineering

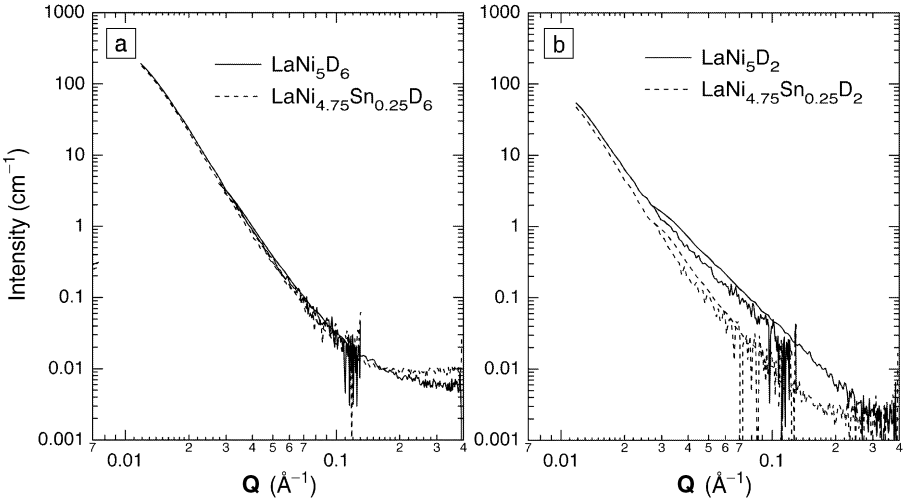

*Figure 5. (a) Porod plot of the measured small-angle neutron scattering (SANS) intensity from the first full deuterium charging of $LaNi_5$ and $LaNi_{4.75}Sn_{0.25}$. **Q** is the scattering vector. (b) Porod plot of the measured SANS intensity from the first full deuterium desorption to 33% absorption (H/unit cell = 2.0) for $LaNi_5$ and $LaNi_{4.75}Sn_{0.25}$. For both plots, the intensities at the highest values of **Q** are dominated by incoherent scattering. The change in slope of the SANS profile in Figure 5b from $\mathbf{Q}^{-4}$ to $\mathbf{Q}^{-3}$ indicates that the hydride zones in $LaNi_{4.75}D_2$ have a two-dimensional character. (After Reference 21.)*

Table II: Energy Storage and Conversion Applications for Metal Hydrides (MH_x) Involving Gas-Phase Reactions.

Application	Required MH_x Attributes	Other Important Issues	Candidate Metal Alloys
Stationary fuel storage	P_{des}[a] ~ 1–10 bar, very low cost, use waste heat, H capacity > 2 wt%	Safety, activation, contamination, degradation	TiFe, V alloys, Mg alloys, AB_2 alloys
Vehicular fuel storage (internal combustion/fuel cells)	H capacity > 5 wt%, low cost, P_{des} ~ 1–10 bar, use waste heat, fast kinetics, durability during cycling, safety, resistance to contamination	Activation, operating temperature range	AB_2, Mg alloys, alanates (TiFe, AB_5 used in the past, but H capacities too low)
Chemical heat pumps and refrigerators	Very fast kinetics, low cost, H capacity, P_{des} ~ 1–5 bar, use waste heat	Hysteresis, degradation during cycling, safety	AB_5, AB_2, AB
Purification, chemical separation, isotope separation (fusion energy)	Fast kinetics, ease of activation, resistance to impurities, reaction efficiency, stability, durability, safety	Cost, operating temperature range, pressure range, radiation effects (i.e., tritium)	Pd, U, V alloys, Zr alloys (AB_2, AB)
Reversible gettering (vacuum systems)	Very low pressure, fast kinetics, pumping speed, ease of activation, durability	Safety, cost, operating temperature range, retention of reversibility	U, Zr alloys (AB_2, AB, $A_xB_yO_z$)
Gas-gap thermal switches	P_{des} < 0.05 bar, fast kinetics, low power (~10 W), durability during temperature cycling, resistance to contamination	Activation, cost, safety, stability, reliability	ZrNi, U, Zr alloys (AB_2, $A_xB_yO_z$)
Compressors (up to ~500 bar) for liquefaction or filling high-pressure gas-storage tanks	Thermal efficiency ($\Delta P/\Delta T$ ratio), fast kinetics, cycling stability, safety, low cost	Contamination, power, equipment complexity (multiple staging MH_x beds), scalability	V alloys, AB_5, AB_2, AB
Sorption cryocoolers (space flight applications)	$\Delta P/\Delta T$ ratio, fast kinetics, cycling stability, P_{abs}[b] ~ constant across absorption plateau, safety, power, reliability	Activation, contamination (acts as source at the cold stage to cause blockage in flow by condensed impurity gases)	$LaNi_{4.8}Sn_{0.2}$, V alloys, AB_5, AB_2, ZrNi

Note: Compiled from References 1, 2, 5, 6, and 27.
[a] P_{des} is the average desorption pressure.
[b] P_{abs} is the average absorption pressure.

problems with the control of hydrogen and heat flows were found. During three years in the 1980s, Daimler-Benz successfully operated a fleet of five delivery vans and five T-model passenger cars in Berlin.[23] Hydrogen was stored in these vehicles in beds of the slightly nonstoichiometric AB_2 alloy $Ti_{0.98}Zr_{0.02}Cr_{0.05}V_{0.43}Fe_{0.09}Mn_{1.5}$, with very fast kinetics and a reasonable storage capacity of 1.8 wt%. However, the most daunting (and still unsolved) problems involve costs (of materials and the appropriate hydride-storage containers) and the very low mass fraction of hydrogen in the storage system, typically 1–2 wt%. While no inexpensive and low-mass hydride system has yet been found for hydrogen-powered automobiles, in the last few years both Mazda [with its Demio FCEV (fuel-cell electric vehicle) station wagon] and Toyota (with its RAV4 EV sport-utility vehicle) have demonstrated fuel-cell-powered prototypes using metal hydride storage.[24] Industrial and mining vehicles, for which storage mass is less of an issue than safe operation within confined spaces, offer a near-term opportunity for a practical fuel-cell/metal hydride system. Figure 6 shows a fuel-cell-powered John Deere Gator vehicle,[25] modified by Westinghouse Savannah River Co. and Energy Partners, that stores hydrogen in beds of $TiFe_{0.9}Mn_{0.1}$.

As indicated in Table II, there are many other situations where metal hydrides are useful and practical.[2] For example, the heat ΔQ from the reversible reaction in Equation 1 can be efficiently used for either heat pumps or refrigeration.[2,26] A lesser-known application for low-pressure metal hydrides is in reversible gas-gap thermal switches to manage heat and power usage in various devices.[27] Finally, closed-cycle Joule–Thomson (J–T) cryogenic refrigerators, commonly called sorption cryocoolers, use metal hydrides to compress and circulate hydrogen. Operation of the sorption compressor is an intermittent process, with desorption of high-pressure (~50–100 bar) hydrogen gas from a hot (i.e., ~400–500 K) hydride bed alternating with absorption from a cool (i.e., 260–300 K) hydride bed. Continuous refrigeration is achieved by the sequential phasing of heating and cooling several sorbent beds (e.g., 3–6) that allow gas to flow to the inlet of the J–T

Figure 6. A John Deere Gator utility vehicle modified by Westinghouse Savannah River Co. and Energy Partners to operate with proton-exchange membrane (PEM) fuel cells and hydrogen gas stored in hydride beds (the cylinders mounted in front of the rear wheel). (After Reference 25.)

valve and the evaporated gas to return to the beds. Sorption cryocoolers are being developed for space flight missions.[28,29] Figure 7 shows the BETSCE (brilliant-eyes ten-kelvin sorption cooler experiment) hydrogen-sorption cryocooler, mounted on the bay wall of the space shuttle Endeavor prior to flight in May 1996. During flight, the BETSCE generated first liquid hydrogen (T = 27 K), then solid hydrogen (T = 11 K). It should be noted that the costs of hydride materials are generally insignificant compared with the total funding of space missions, but performance parameters are at a premium if a space system is to meet its objectives.

In summary, metal hydrides have a long, if not entirely successful, history in energy storage and conversion technologies. Through alloy selection and substitution, many properties can be significantly modified to provide major improvements. Nevertheless, complete optimization with respect to costs and performance has remained elusive. The "Holy Grail" hydride has not yet been found.

Figure 7. BETSCE (brilliant-eyes ten-kelvin sorption cooler experiment) hydrogen-sorption cryocooler mounted on the bay wall of the space shuttle Endeavor prior to flight in May 1996. Metal hydride sorbent beds containing $LaNi_{4.8}Sn_{0.2}H_x$ and $ZrNiH_x$ (hidden by radiators behind the technician) were used to produce first liquid hydrogen (T = 27 K), then solid hydrogen (T = 11 K) in the cryostat (covered by the blanket with the JPL logo).

Acknowledgments

Dr. Charles K. Witham of the Jet Propulsion Laboratory contributed to much of the work reported here. Dr. Witham died from injuries suffered in a bicycle accident on August 5, 2002. The field of hydride research is left poorer by this tragic loss of a young scientist.

The Jet Propulsion Laboratory is operated by the California Institute of Technology under a contract with the National Aeronautical and Space Administration. B. Fultz acknowledges support from U.S. Department of Energy Basic Energy Sciences grant DE-FG03-00ER15035.

References

1. J.J. Reilly, *Z. Phys. Chem. NF* **117** (1979) p. 155.
2. P. Dantzer, in *Hydrogen in Metals III: Topics in Applied Physics,* Vol. 73, edited by H. Wipf (Springer, Berlin, 1997) p. 279.
3. R.B. Schwarz, *MRS Bull.* **24** (11) (1999) p. 40.
4. S. Orimo and H. Fujii, *Appl. Phys. A* **72** (2001) p. 167.
5. S. Suda and G. Sandrock, *Z. Phys. Chem.* **183** (1994) p. 149.
6. G. Sandrock, *J. Alloys Compd.* **293–295** (1999) p. 877; IEA/DOE/SNL Hydride Databases, http://hydpark.ca.sandia.gov/ (accessed July 2002).
7. L. Schlapbach, in *Hydrogen in Intermetallic Compounds II: Topics in Applied Physics,* Vol. 67, edited by L. Schlapbach (Springer, Berlin, 1992) p. 15.
8. D. Richter, R. Hempelmann, and R.C. Bowman Jr., in *Hydrogen in Intermetallic Compounds II: Topics in Applied Physics,* Vol. 67, edited by L. Schlapbach (Springer, Berlin, 1992) p. 97.
9. P. Spatz, H.A. Aebischer, A. Krozer, and L. Schlapbach, *Z. Phys. Chem.* **181** (1993) p. 393.
10. R.C. Bowman Jr., C.H. Luo, C.C. Ahn, C.K. Witham, and B. Fultz, *J. Alloys Compd.* **217** (1995) p. 185.
11. G. Friedlmeier, A. Manthey, M. Wanner, and M. Groll, *J. Alloys Compd.* **231** (1995) p. 880.
12. M. Wanner, G. Hoffmann, and M. Groll, in *Hydrogen Power: Theoretical and Engineering Solutions,* edited by T.O. Saetre (Kluwer Academic Publishers/Academic Press, Dordrecht, 1998) p. 257.
13. H.-H. Lee and J.-Y. Lee, *J. Alloys Compd.* **202** (1993) p. 23.
14. S. Luo, T.B. Flanagan, and P.H.L. Notten, *J. Alloys Compd.* **239** (1996) p. 214.
15. W. Luo, J.D. Clewley, T.B. Flanagan, and W.A. Oates, *J. Alloys Compd.* **185** (1992) p. 321.
16. M. Bououdina, H. Enoki, and E. Akiba, *J. Alloys Compd.* **281** (1998) p. 290.
17. D. Sun, J.M. Joubert, M. Latroche, and A. Percheron-Guégan, *J. Alloys Compd.* **239** (1996) p. 193.
18. M. Bououdina, J.-L. Soubeyroux, and D. Fruchart, *J. Alloys Compd.* **327** (2001) p. 185.
19. T. Sakai, M. Matsuoka, and C. Iwakura, in *Handbook on the Physics and Chemistry of Rare Earths,* Vol. 21, edited by K.A. Gschneidner Jr. and L. Eyring (Elsevier, Amsterdam, 1995) p. 133.
20. P.H.L. Notten, in *Interstitial Metallic Alloys,* NATO Ser. Vol. 281, edited by F. Grandjean, G. Long, and K.H.J. Buschow (Kluwer Academic Publishers, London, 1995) p. 151.
21. B. Fultz, C.K. Witham, and T.J. Udovic, *J. Alloys Compd.* **335** (2002) p. 165.
22. B.V. Ratnakumar, C. Witham, R.C. Bowman Jr., A. Hightower, and B. Fultz, *J. Electrochem. Soc.* **143** (1996) p. 2578.
23. J. Toepler and K. Feucht, *Z. Phys. Chem. NF* **164** (1989) p. 1451.
24. A.J. Appleby, *Sci. Am.* **281** (1) (1999) p. 74.
25. T. Motyka, W.A. Summers, and L.K. Heung, "Industrial Fuel-Cell Vehicles with Metal Hydride Storage," in *Proc. 11th Canadian Hydrogen Conf.* [CD-ROM] (Canadian Hydrogen Association, Toronto, 2001) Paper No. 8C-#10.
26. E. Willers and M. Groll, *Int. J. Refrig.* **22** (1999) p. 47.
27. M. Prina, J.G. Kulleck, and R.C. Bowman Jr., *J. Alloys Compd.* **330–332** (2002) p. 886.
28. S. Bard, P. Karlmann, J. Rodriguez, J. Wu, L. Wade, P. Cowgill, and K.M. Russ, in *Cryocoolers,* Vol. 9, edited by R.G. Ross Jr. (Plenum Publishers, New York, 1997) p. 567.
29. L.A. Wade, P. Bhandari, R.C. Bowman Jr., C. Paine, G. Morgante, C.A. Lindensmith, D. Crumb, M. Prina, R. Sugimura, and D. Rapp, in *Advances in Cryogenic Engineering,* Vol. 45, Q.-S. Shu, chief editor (Kluwer Academic/Plenum Publishers, New York, 2000) p. 499. □